Peer-reviewed version available at Entropy 2018, 20, 557; doi:10.3390/e20080557

Article

Magnetocaloric effect in non-interactive electrons systems: "The Landau problem" and its extension to quantum dots

Oscar A. Negrete [1,*], Francisco J. Peña [1], Juan M. Florez [1], and Patricio Vargas [1,4]

[1] Departamento de Física, Universidad Técnica Federico Santa María, Valparaíso, Chile; oscar.negrete@gmail.com ; f.penarecabarren@gmail.com; juanmanuel.florez@usm.cl patricio.vargas@usm.cl

[4] Centro para el Desarrollo de la Nanociencia y la Nanotecnología, CEDENNA, Santiago, Chile

* Correspondence: oscar.negrete@usm.cl

Abstract: In this work, we report the magnetocaloric effect (MCE) in two systems of non-interactive particles, the first corresponds to the Landau problem case and the second, the case of an electron in a quantum dot subjected to a parabolic confinement potential. In the first scenario, we realize that the effect is totally different from what happens when the degeneration of a single electron confined in a magnetic field is not taken into a ccount. In particular, when the degeneracy of the system is negligible, the magnetocaloric effect cools the system, while in the other case, when the degeneracy is strong, the system heats up. For the second case, we study the competition between the characteristic frequency of the potential trap and the cyclotron frequency to find the optimal region that maximizes the ΔT of the magnetocaloric effect, and due to the strong degeneration of this problem, the results are in coherence with those obtained for the Landau problem. Finally, we consider the case of a transition from a normal MCE to an inverse one and back to normal as a function of temperature. This is due to the competition between the diamagnetic and paramagnetic response when the electron spin in the formulation is included.

Keywords: Magnetocaloric Effect; Magnetic cycle; Thermodynamics.

1. Introduction

From a fundamental point of view, the magnetocaloric effect (MCE) consists of the temperature variation of a material due to the variation of a magnetic field to which it is subjected. The MCE was observed for the first time by Warburg in 1881 [1] but it was until 1918 that Weiss and Picard [2] exposed the physical principles that govern this phenomenon, thus allowing Debye [3] in 1926 to propose the first practical applications. A year later Giauque [4] designs magneto-thermal cycles in order to explore physical phenomena at temperatures close to the liquefaction point of helium (4.2K). A little later in 1933, Giauque and Mac Dougall [5] reached temperatures of the order of 250 mK with paramagnetic salts exceeding for the first time in history the 1K barrier. For more than four decades the magnetic refrigeration was confined solely to the scientific scope, never arriving thus to make the technology of domestic use, this due to the low work temperature of the magnetocaloric materials. All the compounds are known at that date only work at temperatures of the order of 5 K, making it impossible to use them in less extreme conditions. It was not until 1976 that Brown [6], working with a prototype of magnetic cooler using Gadolinium as the active compound, showed that it was feasible to have a refrigerating machine at room temperature. Pecharsky and Gschneider [7] discovered in 1997 a series of materials with amazing magnetocaloric responses thus enabling the implementation of magnetothermic machines that were previously not considered feasible due to the low working temperatures. Nowadays the research of the MCE effect reawakens a strong interest in the scientific community again [8–28].

Compounds with working temperatures increasingly closer to room temperature are being studied all over the world with the hope of finally finding a suitable candidate, and thus replacing the current refrigeration technology by a more efficient alternative and compatible with current environmental emergencies and requirements.

In physical terms, the MCE is closely linked to the behaviour of the total entropy (S) since there is a connection between the temperature changes that a system experiences together with entropy variations. In this context, in a recent work [29], the study of the degeneracy role in the Landau problem shows a very interesting behaviour for the magnetic field along an isoentropic stroke compared with the calculation in his absence. The low-temperature response of the entropy in the Landau problem it is only proportional to the amplitude of the external magnetic field, so the variation of S is a good candidate to study the MCE for this case. Nowadays it is physically possible to confine electrons in two dimensions (2D). For instance, quantum confinement can be achieved in semiconductor heterojunctions, such as GaAs and AlGaAs. At room temperature, the bandgap of GaAs is 1.43 eV while it is 1.79 eV for AlxGa1-x As ($x = 0.3$). Thus, the electrons in GaAs are confined in a 1-D potential well of length L in the z-direction. Therefore, electrons are trapped in 2D space, where a magnetic field along z-axis can be applied [30].

On the other hand, a more realistic approach can be given if we consider an ensemble of non-interacting electrons trapped in a quantum dot, this due to the control that can be achieved regarding the number of electrons that each quantum dot can have individually. Moreover, the advances in technology allow these systems to work below $T = 1\ K$ in temperature [31–34].

In this work, we report the MCE effect for two systems, the first one correspond to the case of the very well know Landau problem considering the degeneracy effects in their energy levels and in the second one, the case of an electron in a quantum dot subjected to a confining potential modelled as a parabolic potential in two dimensions who is the standard approach to semiconductor quantum dots. This study is based on the fact that thermodynamics for this system can be solved by the exact calculation of the partition function, the free energy, the entropy, in such a way that the variation of the temperature with the magnetic field can be thoroughly analysed. In particular, we found that the effect of degeneracy in the energy levels for the Landau problem modifies the magnetocaloric effect from normal to an inverse case. For an electron trapped in a quantum dot, we treat the different scenarios that were obtained due to the competition between the cyclotron frequency and the frequency related to the intensity of the parabolic trap inside the dot, finding a good inverse MCE in concordance to our results obtained for the highly degenerated Landau problem. Finally, to reinforce the idea of the role of the degeneracy on energy levels on the MCE, we consider the electron spin, thus including cases with Zeeman energy. As a consequence, there is now a competition between the diamagnetic and paramagnetic effects. This allows us to explore a broader range for the intensity of the controllable external magnetic field. Due to the splitting of energy levels and therefore a decrease in the energy levels degeneration, we found MCE transitions from normal to inverse to normal form, for a particular range of temperatures and characteristic cyclotron frequency.

2. Model

We consider the case of an electron with an effective mass m^* and charge e placed in a magnetic field B, where the Hamiltonian of this problem working in the symmetric gauge leads to the known expression (the Landau problem):

$$\hat{H} = \frac{1}{2m^*}\left[\left(p_x - \frac{eBy}{2}\right)^2 + \left(p_y + \frac{eBx}{2}\right)^2\right], \tag{1}$$

Preprints (www.preprints.org) | NOT PEER-REVIEWED | Posted: 2 July 2018 doi:10.20944/preprints201807.0010.v1

Peer-reviewed version available at Entropy 2018, 20, 557; doi:10.3390/e20080557

where we use the minimal coupling given by $\vec{p} \to \vec{p} + e\vec{A}$, being $\vec{A}$ the magnetic vector potential. The solution for the eigenvalues of energies, that is obtained solving the Schrödinger equation, are the corresponding Landau levels of energy, whose expression is given by

$$\mathcal{E}_n = \hbar\omega_B \left(n + \frac{1}{2}\right). \tag{2}$$

Here, $n = 0, 1, 2,$...is the quantum number, and

$$\omega_B = \frac{eB}{m^*} \tag{3}$$

is the standard definition for the cyclotron frequency [35–38]. With the definition of the parameter ω_B, we can define the Landau radius that captures the effect of the intensity of the magnetic field, given by $l_B = \sqrt{\hbar/(m^*\omega_B)}$. The energy spectrum for each level is degenerate with a degeneracy $g(B)$ given by [38]

$$g(B) = \frac{eB}{2\pi\hbar}\mathcal{A}, \tag{4}$$

with $\mathcal{A}$ being the area of the box perpendicular to the magnetic field B. So, with this approach it is straightforward to calculate the partition function for the Landau problem, and it turns out to be

$$\mathcal{Z}_L = \frac{m^*\omega_B\mathcal{A}}{4\pi\hbar}\text{csch}\left(\frac{\beta\hbar\omega_B}{2}\right), \tag{5}$$

which corresponds to standard partition function for a harmonic oscillator in the canonical ensemble, with a degeneracy for level equal to $g(B)$, and β corresponds to the inverse temperature $1/k_BT$. In the Fig. 1, we display a pictorial description of our studied systems.

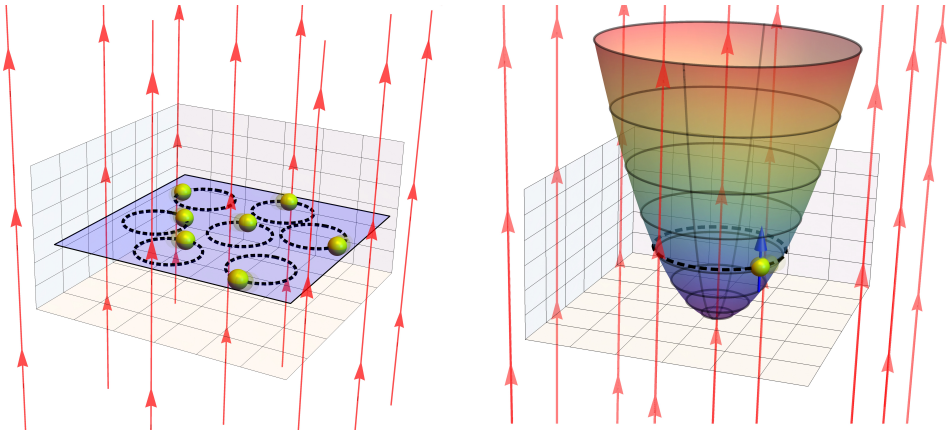

Figure 1. Pictorial representation of the systems. The left panel depicts the Landau problem. We recall that in our formulation we do not consider the edge effects. Red arrows represent the external magnetic field perpendicular to the sample. The right panel depicts an electron with spin (blue arrow) trapped in a parabolic potential that represent an electron in a quantum dot.

Another interesting and highly degenerate problem corresponds to the case of a single electron trapped in a quantum dot whose non-relativistic version can be simply obtained if we modify the Hamiltonian of Eq. (1) by adding a parabolic potential of the form:

$$V(x,y) = \frac{m^*}{2}\omega_d^2\left(x^2 + y^2\right), \tag{6}$$

where ω_d is the frequency associated with the parabolic trap and m^* is the effective mass of the electron (Fig. 1, right panel). In this case, the eigenvalues of energy corresponds to the very well know Fock-Darwin energy levels given by:

$$\mathcal{E}_{n,m} = \hbar\Omega(2n + |m| + 1) - m\frac{\hbar\omega_B}{2}, \tag{7}$$

where $n = 0, 1, 2, ...$ and $m = 0, \pm1, \pm2...$ represent the radial and the azimuthal quantum number respectively. The "effective frequency" Ω is defined in the form

$$\Omega = \sqrt{\omega_d^2 + \frac{\omega_B^2}{4}}, \tag{8}$$

and the effective magnetic length is (or effective landau radius) is given in this case by $l_B = \sqrt{\hbar/(m^*\Omega)}$. The calculation of the exact partition function has been already discussed in previous works [35,36,38]. We highlight the works of Kumar *et al.* [38] and Muñoz *et al.* [36], where the first one calculates the partition function from a functional-integral approach and the second one by substituting the quantum numbers (n, m) for two new integer numbers n_+ and n_-. This two approaches lead to a thermodynamical system characterized by two frequencies, called ω_+ and ω_-, given by the expression:

$$\omega_\pm = \Omega \pm \frac{\omega_B}{2}, \tag{9}$$

and the partition function has the following form:

$$\mathcal{Z}_d = \frac{1}{4}\text{csch}\left(\frac{\hbar\beta\omega_+}{2}\right)\text{csch}\left(\frac{\hbar\beta\omega_-}{2}\right). \tag{10}$$

Note that the partition function has a divergence when $\omega_d \to 0$, but none of the thermodynamic quantities which are expressed as derivatives of $\mathcal{Z}_d$, suffer from this problem. On the other hand, it happens that the entropy, obtained from the Eq. (10), diverges for $\omega_d \to 0$, but we recall that this case represents a quantum harmonic oscillator of zero frequency, due to the fact that when $\omega_d \to 0$ we have $\omega_- \to 0$, and it does not represent a real physical system.

To obtain a more precise calculation especially when we consider the case of strong magnetic fields for the electron trapped in a quantum dot, we also take into account the electron spin of value $\frac{\hbar\hat{\sigma}}{2}$ and magnetic moment μ_B, where $\hat{\sigma}$ is the Pauli spin operator and $\mu_B = \frac{e\hbar}{2m^*}$. Here the spin can have two possible orientations, one is $\uparrow$ or $\downarrow$ with respect to the applied external magnetic field B in the direction of the z-axis. Therefore, we need to add the Zeeman term in the Fock-Darwin energy levels Eq. (7). Consequently, the new energy spectrum is given by:

$$\mathcal{E}_{n,m,\sigma} = \hbar\Omega(2n + |m| + 1) - m\frac{\hbar\omega_B}{2} - \mu_B\sigma B. \tag{11}$$

The partition function for this case include only one additional term as compared to the one given in Eq. (10) and is given by:

$$\mathcal{Z}_{dS} = \frac{1}{2}\text{csch}\left(\frac{\hbar\beta\omega_+}{2}\right)\text{csch}\left(\frac{\hbar\beta\omega_-}{2}\right)\cosh\left(\frac{\hbar\beta\omega_B}{2}\right). \tag{12}$$

It is important to mention that this partition function, Eq. (12), includes two physical effects associated to the electron trapped in the quantum dot, the diamagnetic response associated to the "csch" terms, and the paramagnetism in the "cosh" term.

2.1. Magnetocaloric Observables

To understand the expressions that we use to describe the MCE, we can think in a general non-deformable system under the action of an external magnetic field of intensity B at a temperature T, which magnetothermic properties can be extracted using the free energy of Gibbs G. Hence, we can define the specific heat at a constant magnetic field as the second partial derivative of G with respect to temperature T

$$C_B = -T\left(\frac{\partial^2 \mathrm{G}}{\partial T^2}\right)_B. \tag{13}$$

Having knowledge of how the heat is transferred between the material and its environment, is essential to understand and optimize the efficiency of the thermal machines and other systems that require the generation of temperature gradients. C_B could give us further insights into such processes as well as to witness phase transitions between different magnetic orders as a function of different external or intrinsic parameters.

We emphasize that we work here with an entropy S as function of state that depends only of two thermodynamical variables, thus we have $S \equiv S(T, B)$. This allows us to write the total differential expression for the entropy,

$$dS(B,T) = \left(\frac{\partial S}{\partial B}\right)_T dB + \left(\frac{\partial S}{\partial T}\right)_B dT. \tag{14}$$

From Eq. (14) we can now derivate the magnetocaloric expressions which arise from considering two thermodinamical paths, i.e., an adiabatic and an isothermal ones. Correspondingly, for the adiabatic paths, we can make the Eq. (14) equal to zero. Using then the relation given by $\left(\frac{\partial^2 \mathrm{G}}{\partial T^2}\right)_B = -\left(\frac{\partial S}{\partial T}\right)_B$ in the Eq. (13) for the specific heat and the Maxwell relation $\left(\frac{\partial \mathrm{M}}{\partial T}\right)_B = -\left(\frac{\partial S}{\partial B}\right)_T$, where the magnetization of the system has the form $M(T,B) = -\left(\frac{\partial \mathrm{G}}{\partial B}\right)_T$, we can obtain the adiabatic change in the temperature ΔT for the system respect to the variations of the external magnetic field, such expression is given by

$$\Delta T = -\int_{B_i}^{B_f} \frac{T}{C_B}\left(\frac{\partial M}{\partial T}\right)_B dB. \tag{15}$$

For the isothermal path we can obtain from the Eq. (14) that the change of entropy between two magnetic field is given by

$$\Delta S = \int_{B_i}^{B_f}\left(\frac{\partial M}{\partial T}\right)_B dB \tag{16}$$

Moreover, we can obtain the change in the entropy for a trajectory with a constant magnetic field (i. e. isomagnetic strokes) from Eq. (14)

$$\Delta S = \int_{T_i}^{T_f}\left(\frac{C_B}{T}\right) dT \tag{17}$$

Now, there are two different paths for the magnetothermic cycles for the degenerate and non-degenerate cases of the Landau problem, respectively, that we describe in the Fig. 2. This two cases arise for the very noticeable difference in the behaviour of the adiabatic trajectories discussed previously in the Ref [29]. Specifically, when we make the Eq. (14) equal to zero, we can construct a differential equation relating the magnetic field and the temperature for adiabatic processes in the scenario of a degeneration, which has the form:

$$\frac{dB}{dT} = -\frac{C_1^2 \frac{B^2}{T^3}\mathrm{csch}^2\left(C_1 \frac{B}{T}\right)}{\frac{1}{B} - C_1^2 \frac{B}{T^2}\mathrm{csch}^2\left(C_1 \frac{B}{T}\right)}, \tag{18}$$

Preprints (www.preprints.org) | NOT PEER-REVIEWED | Posted: 2 July 2018 doi:10.20944/preprints201807.0010.v1

Peer-reviewed version available at Entropy 2018, 20, 557; doi:10.3390/e20080557

where C_1 is a constant given by $C_1 = \frac{e\hbar}{2k_B m^*}$. This previous equation has an analytical solution given by

$$C_1 \frac{B}{T} \coth\left(C_1 \frac{B}{T}\right) + \ln\left(C_1 B\right) - \ln\left[\sinh\left(C_1 \frac{B}{T}\right)\right] = \mathcal{C}_2, \tag{19}$$

where $\mathcal{C}_2$ is an integration constant. Note that the additional term in the differential equation which provides the degeneracy, $g(B)$, is the factor $(1/B)$ in the dominator of Eq. (18). If this term vanishes, the differential equation has a simpler form $\frac{dB}{dT} = \frac{B}{T}$ with a linear dependence between the changes of the magnetic field and the temperature, correspondingly. Because of this, we explain these two different cases separately and propose an schematic representation of the cycles for a better understanding.

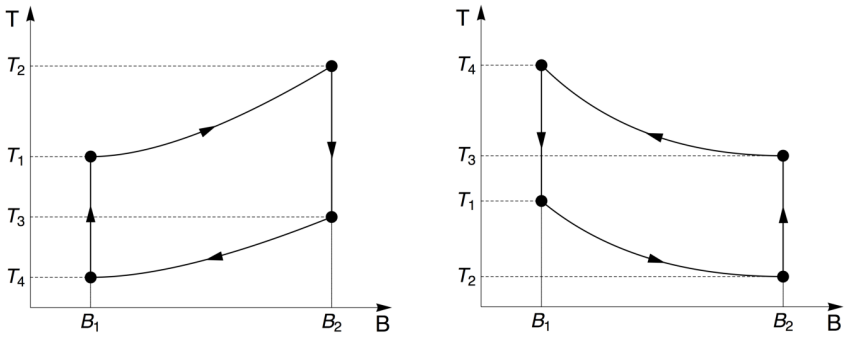

Figure 2. General ideal description of the MCE. Left panel: Standard MCE, we start with our system a $T = T_1$ and $B = B_1$, by performing an adiabatic stroke to $B = B_2$ the system heats up reaching $T = T_2$ (due to the increase of the system phonons entropy), the system is in contact with a thermal reservoir reaching a temperature of $T = T_3$, now we proceed with an adiabatic demagnetization stroke back to $B = B_1$, therefore the system cools down to $T = T_4$, then the system is in contact with a sample to cool down, therefore our system reaches again a temperature $T = T1$. Right panel: Inverse MCE, we start with our system a $T = T_1$ and $B = B_1$, by performing an adiabatic stroke to $B = B_2$, the system cools down to $T = T_2$ (this is due to the decrease of the system phonons entropy), here the system is in contact with a sample to cool down, therefore our system reaches $T = T_3$, now we proceed with an adiabatic demagnetization stroke back to $B = B_1$, therefore the system now heats up to $T = T_4$, the system is in contact with a thermal reservoir, therefore reaching again a temperature $T = T_1$.

Non-degenerate case: In this case, (Fig. 2, left panel) the system, having a temperature (T_1), is magnetized adiabatically, therefore the final temperature (T_2) is greater than the initial one $(T_2 > T_1)$. At this point, the system is put in contact with a cold reservoir so that it reaches a lower temperature $(T_3 < T_2)$, from there, an adiabatic demagnetization occurs, cooling the system again reaching a final temperature (T_4) which less than the initial temperature $(T_4 < T_1)$. Here we use a system to cool a sample (gas or solid material) then reaching the system a final temperature $(T_5 = T_1$ (theoretically)) and therefore our magnetic system is heated up again beginning with the initial temperature (T_1) and a new cycle starts.

Degenerate case: In this case, (Fig. 2, right panel) our magnetic system is at temperature T_1 where we subject the system to an adiabatic magnetization, the system reaches a temperature $T_2 < T_1$, at this moment we use our system to cool a sample (gas or solid material) therefore this adds heat to our magnetic system reaching a temperature of T_3 $(T_3 > T_2 > T_1)$, now we start from here doing an adiabatic demagnetization process, therefore reaching our system a final temperature of T_4 higher than the temperature T_3, at that moment the system should be put in contact with a reservoir at temperature T_1 or less in order to reach quickly that temperature, so that the cycle can be started again and thus we are able to cool a material.

For the case of an electron trapped in a quantum dot, we treat two instances, the case with an without an intrinsic spin. We report that, if we do not consider the Zeeman effect, the system responds like in the degenerate case of the Landau problem. When the Zeeman term is taken into account, the systems experiment both direct and inverse MCE.

It is important to recall that in our thermodynamic analysis, all the thermal quantities are derived from the partition function $\mathcal{Z}$. In the generic form:

$$S(T,B) = k_B T \left(\frac{\partial \ln \mathcal{Z}}{\partial T}\right)_B, \tag{20}$$

$$C_B = \left(\frac{\partial U}{\partial T}\right)_B, \tag{21}$$

where $U = k_B T^2 \left(\frac{\partial \ln \mathcal{Z}}{\partial T}\right)_B$ and finally

$$M = k_B T \left(\frac{\partial \ln \mathcal{Z}}{\partial B}\right). \tag{22}$$

3. Results and discussion

3.1. Landau Problem: Influence of energy degeneracy on the MCE .

From Eq. 5 we straightforwardly calculate the thermodynamic quantities for the non degenerate case. First we analyse the MCE starting with the corresponding thermodynamic entropy, which is given by

$$S(T,B) = \frac{\hbar\omega_B}{2T} \coth\left(\frac{\beta\hbar\omega_B}{2}\right) + k_B \ln\left[\operatorname{csch}\left(\frac{\beta\hbar\omega_B}{2}\right)\right] \tag{23}$$

The entropy as a function of the temperature shows two behaviours. First, it grows as a function of the temperature and second, it decreases at a fixed temperature when the intensity of external magnetic field increases as we show in the left panel of Fig. 3. If we consider an isoentropic trajectory, represented for example by a straight horizontal line in the Fig. 3, as the magnetic field increases the different curves of the entropy, cut the straight horizontal line in at successively higher temperatures. This explains the linearity that we obtain from the solution of the trivial differential equation of first order given in the Eq. (18) when we don't have the extra term $1/B$ in the denominator of the same equation. In the right panel of Fig. 3, we observe that for all temperature range the values for $-\Delta S$ are positive, so we expect a normal MCE as we see in the Fig. 4 with corresponding positive values for ΔT. In real low dimensional systems just small changes of temperature are often achieved. If we use the above argument that would mean that usual work temperatures are also small, as indeed they are. To obtain a realistic values for ΔT, we need to work at low temperatures. This is a consequence of the linear relationship between B and T in the adiabatic paths for this ideal system. The physical reason for that is we are dealing with an ideal and perfect diamagnetic system.

Preprints (www.preprints.org) | NOT PEER-REVIEWED | Posted: 2 July 2018 doi:10.20944/preprints201807.0010.v1

Peer-reviewed version available at Entropy 2018, 20, 557; doi:10.3390/e20080557

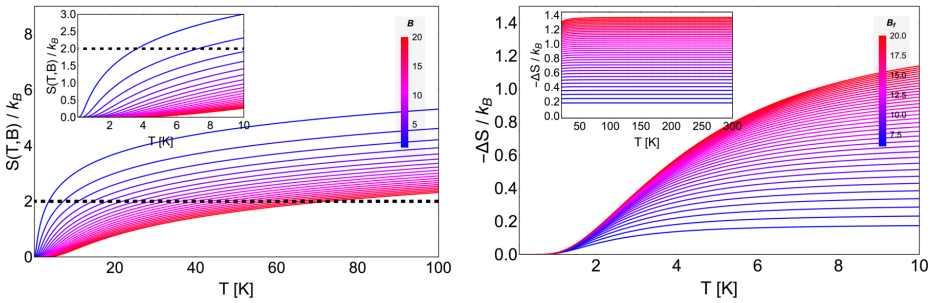

Figure 3. Left panel: Entropy (in k_B units) for the non-degenerate case of the Landau problem, as function of temperature (in Kelvin) and for different values of external magnetic field intensity (measured in Tesla) from 0.1 T to 20 T. The straight horizontal line represents the adiabatic line $S(T,B)/k_B = 2$, cutting different magnetic fields entropies at different temperatures. The inset shows the entropy in the temperature range from $T = 0$ K to $T = 10$ K.
Right Panel: Entropy change, ΔS, according to Eq. (16), as a function of the temperature for the non-degenerate case, where $\Delta B = B_f - B_i$. We display this figure with an initial value of the external magnetic field of $B_i = 5$ T to B_f (from 5.01 T to 20 T) and for temperatures from $T = 2$ K to $T = 10$ K. The inset depicts the values for ΔS from $T = 40$ K to $T = 300$ K.

The magnetization for the non-degenerate case is simply given by the expression:

$$M(T,B) = -\mu_B \coth\left(\frac{\hbar\omega_B}{2k_B T}\right), \tag{24}$$

where $\mu_B = e\hbar/2m^*$ is the Bohr magneton. We plot this magnetization behaviour in the inset figure of Fig. 4 in the range of low temperature and low magnetic fields. As can be seen, the absolute value of the magnetization decreases as the external magnetic field increases. The explanation of this conduct is the diamagnetic response. We need to remember that we have spinless electrons, so the magnetization is associated to a circular constant current I (charge times velocity) of section A in the form of $M \sim IA$, where A can be written as

$$A = \pi l_B^2, \tag{25}$$

where l_B is the Landau radius. So, the higher the magnetic field, the smaller the effective area A is, in order to localize the electron in a smaller region in the space and vice-versa. Therefore, the magnetization decreases by increasing the external magnetic field as we see in the inset of Fig. 4.

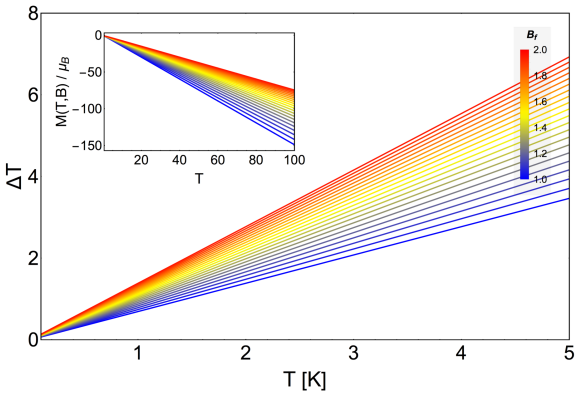

Figure 4. MCE for the non-degenerate case of the Landau problem as a function of temperature .We display ΔT with an initial value of the external magnetic field $B_i = 0.5$ T to B_f from 1 T (blue) to 2 T (red). The inset shows the values for $M(T,B)$ for external magnetic fields ranging from $B = 1$ T to $B = 2$ T.

Preprints (www.preprints.org) | NOT PEER-REVIEWED | Posted: 2 July 2018 doi:10.20944/preprints201807.0010.v1

Peer-reviewed version available at Entropy 2018, 20, 557; doi:10.3390/e20080557

The effect of the degeneracy in the energy levels of the Landau problem modify all the results previously presented. The entropy for this case is given by

$$S_L(T,B) = \frac{\hbar\omega_B}{2T}\coth\left(\frac{\beta\hbar\omega_B}{2}\right) + k_B \ln\left[\frac{g(B)}{2}\mathrm{csch}\left(\frac{\beta\hbar\omega_B}{2}\right)\right], \tag{26}$$

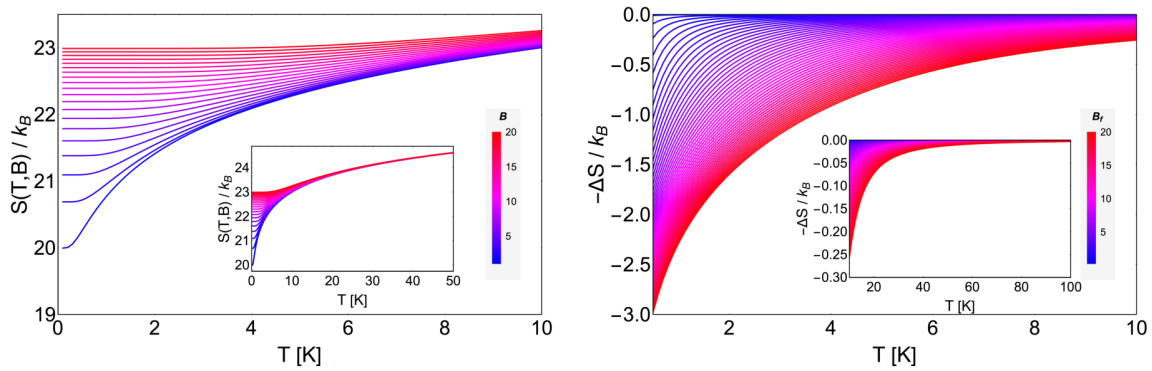

Figure 5. Left panel: Behaviour of the entropy $S_L(T,B)$ for the Landau problem with degeneracy. We show $S_L(T,B)$ in the range of B between 0.1 T to 20 T and for the temperature up to 10 K. (The area used was of $\mathcal{A} \equiv 1\ mm^2$). It is clearly observed that the entropy grows with the magnetic field and approximately collapses to the same value at high temperatures as we see in the inset graphic. Right Panel: ΔS_L for the degenerate scenario of the Landau Problem. We show -$\Delta S_L(T, B_i, B_f)$ in a range of the external magnetic fields, for $B_i = 0.01$ T and $B_f = 0.1$ T to $B_f = 20$ T and up to 10 K in the temperature. Inset figure shows the variation of entropy for a range of temperature between 10 K to 100 K, where clearly observe that the variation of $-\Delta S$ decrease approximately in a factor of 10 as compared to the low temperature behaviour, as expected.

where this expression only differs from the Eq. (23) in the logarithmic term by the additional factor $g(B)/2$. This entropy is shown in the left panel of the Fig. 5, where we clearly see an important feature at low temperature i. e. the entropy of the Landau problem with degeneracy satisfy the following relation:

$$S_L(T,B)_{T\to 0} \equiv S(B) \sim k_B \ln\left(g(B)\right). \tag{27}$$

This entropy depends only on the external magnetic field, and at $T = 0$ simply represents the residual entropy of the ground state. It grows if the intensity of the external field grows, contrary to the non-degenerate case. This can be explained with the fact that for low temperatures the strong linear degeneracy dependence on the field, implies more available states, so consequently, the entropy must increase as field increases. On the other hand, in the high temperature range (see inset on the left panel of Fig. 5) the entropy for different magnetic fields approximately collapses to the same value, but still existing a finite $\Delta S > 0$, allowing the analysis of the MCE at higher temperatures.

Preprints (www.preprints.org) | NOT PEER-REVIEWED | Posted: 2 July 2018 doi:10.20944/preprints201807.0010.v1

Peer-reviewed version available at Entropy 2018, 20, 557; doi:10.3390/e20080557

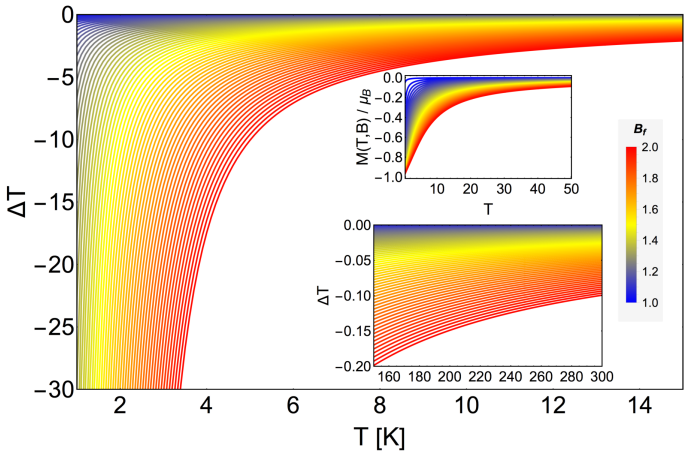

Figure 6. MCE for the Landau problem with degeneration as a function of temperature. The main figure shows ΔT in a range of the external magnetic fields, from $B_f = 1\ T$ to $B_f = 20\ T$ at fixed $B_i = 0.01T$, and up to 15 K in the temperature scale. The upper inset shows the values for $M(T, B)$ for external magnetic fields ranging from $B = 1T$ to $B = 2T$. The lower inset depicts the variation of ΔT for higher temperatures up to 300 K.

As we see in the right panel of the Fig. 5 , we obtain negative values for $-\Delta S$, opposite to the non-degenerate case (see Fig. 3). Therefore when we analyse the MCE for this system, we obtain negative values for ΔT, as presented in Fig. 6. Here, we discuss two possible scenarios, low temperature and high-temperature behaviour for the same range of external magnetic fields. In the case of low temperature, we obtain larger values for ΔT, but it is important to point out that we have only a region of physical validity to avoid negative temperatures. Approximately from a temperature $T \sim 7\ K$ and above it, we can work with all proposed range of magnetic fields (from $B = 0.01\ T$ to $B = 20\ T$) as we see in Fig. 6 , because all the values of ΔT are acceptable (i.e. $T_f = T_i + \Delta T > 0K$). If we decrease the value of the initial temperature T beyond this value, we must proceed carefully. At lower temperature, the physically acceptable solutions cannot take higher values for the external magnetic field in order to avoid final negative temperatures as we clearly appreciate in the Fig. 6.

3.2. MCE for electrons trapped in a quantum dot.

In this section we now develop the case of a electron trapped by a quantum dot. From Eq. (10) it is straightforward to derive the entropy, $S_d(T, B)$, for this problem:

$$\frac{S_d(T,B)}{k_B} = \frac{\hbar\omega_+}{2k_BT}\coth\left(\frac{\hbar\omega_+}{2k_BT}\right) - \ln\left(2\sinh\left(\frac{\hbar\omega_+}{2k_BT}\right)\right) + \frac{\hbar\omega_-}{2k_BT}\coth\left(\frac{\hbar\omega_-}{2k_BT}\right) - \ln\left(2\sinh\left(\frac{\hbar\omega_-}{2k_BT}\right)\right). \tag{28}$$

Fig. 7 shows the entropy, magnetization (from Eq. (22)) and specific heat (from Eq. (21)) as a function of temperature. We clearly appreciate that the entropy function grows with the magnetic field as in the case of the Landau problem with the degeneracy effects. Thence, by calculating -$\Delta S = S(T, B_i) - S(T, B_f)$ with $B_f > B_i$ we obtain negative values. This result is expected due to the strong degeneracy of the Fock-Darwin levels reflected in the dependence of the spectrum of Eq. (7) in the azimuthal quantum number m. The partition function capture this effect when we write the quantum numbers (n, m) in the form of two new numbers (n_+, n_-) in order to form two frequency oscillators given by ω_+ and ω_-.

Preprints (www.preprints.org) | NOT PEER-REVIEWED | Posted: 2 July 2018 doi:10.20944/preprints201807.0010.v1

Peer-reviewed version available at Entropy 2018, 20, 557; doi:10.3390/e20080557

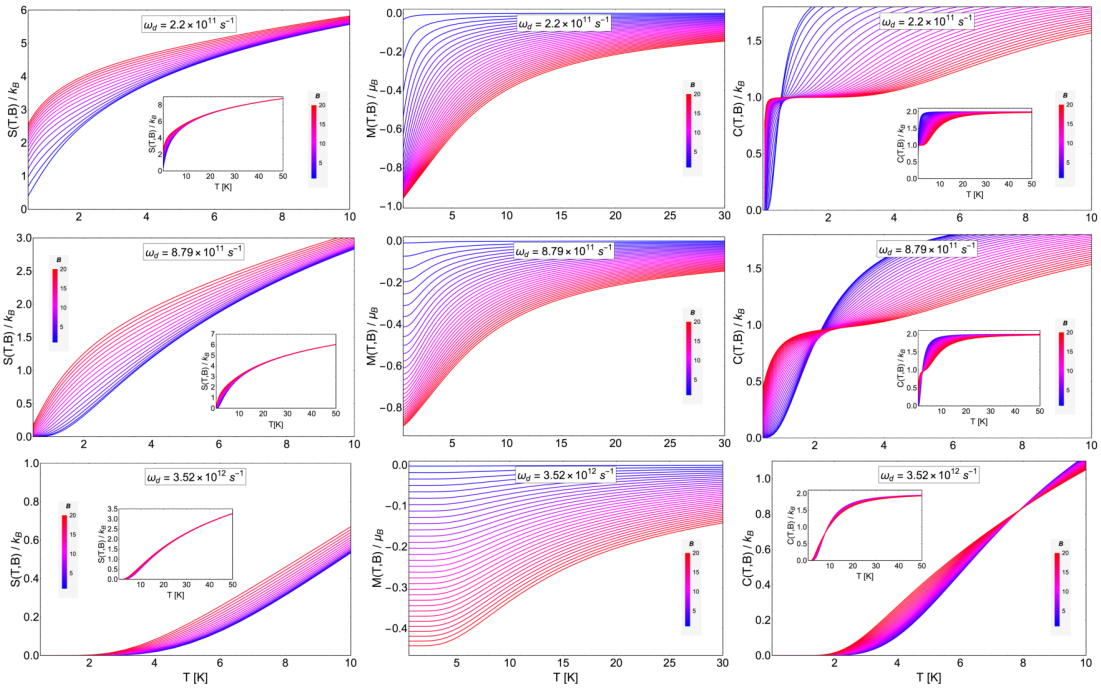

Figure 7. Spinless electrons in a quantum dot. Entropy $S_d(T,B)$ (left panels), $M(T,B)$ (middle panels) and $C_B(T,B)$ (right panels) as function of temperature (T) from 0 K to 10 K for different values of magnetic field in the range of 0.1 T to 20 T. In the middle panels of the graphs, we selected the representative value for the characteristic frequency of the harmonic trap in $\omega_d = 8.7941 \times 10^{11}\ s^{-1}$, which in terms of energy represents an approximately value of 3.6 meV. For the superior panels, we use the value $\frac{\omega_d}{4}$ and in the bottom panels the case of $4\omega_d$ for the characteristic frequency of the dot structure ($\omega_B = 1.76 \times 10^{11} B\ \ s^{-1}$, where B is in Tesla units for comparison).

For the analysis of the ΔS it is convenient to analize the results in three cases due to the competition between ω_d and ω_B. In order to do this, we plot the variation of the entropy as function of temperature for the case of a characteristic dot frequency of $\omega_d = 8.7941 \times 10^{11} s^{-1}$ whose value is associated to a cyclotron frequency for $B = 5\ T$ (i. e. $\omega_B = 1.76 \times 10^{11} B\ \ [C/Kg]$, with B in units of Tesla) of the external magnetic field intensity. Thereby, to analyse the different regions of $-\Delta S$ we plot this quantity in three insets of Fig. 8 using an initial value of external magnetic field of $B_i = 0.01\ T$, $B_i = 4.54\ T$ and $B_i = 5.51\ T$ in the left, center and right panel respectively. This in order to satisfy the three regimes of frequencies. The left panel is associated to a range of final external fields corresponding to B_f between 0.11 T to 4.51 T (i. e. $\omega_d > \omega_B$), the middle panel is associated to a range of final external fields corresponding to B_f between 4.55 T to 5.51 T ($\omega_d \sim \omega_B$) and the right panel for B_f from 5.56 T to 15.55 T (i. e. $\omega_d < \omega_B$). We observe that the magnitude of $-\Delta S$ increase (in absolute value) for higher magnetic fields, as we see from the diagram for $S(T,B)$ of the Fig. 7, and is more notorious in the range of a temperature from $T \sim 2\ K$ to $T \sim 4\ K$.

Preprints (www.preprints.org) | NOT PEER-REVIEWED | Posted: 2 July 2018 doi:10.20944/preprints201807.0010.v1

Peer-reviewed version available at Entropy 2018, 20, 557; doi:10.3390/e20080557

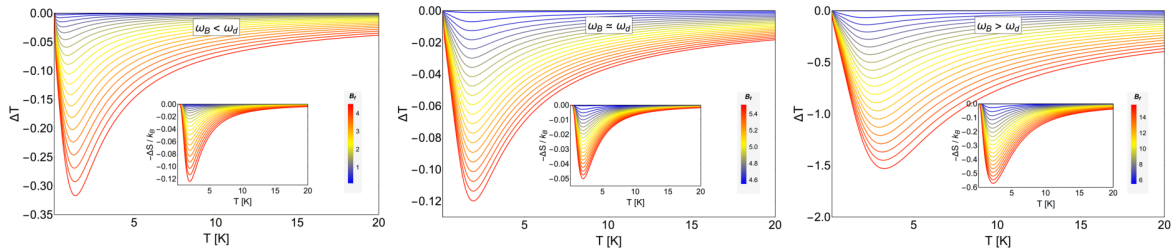

Figure 8. MCE effect for spinless electrons in a quantum dot. ΔT for : i) $\omega_B < \omega_d$ (left panel) ii) $\omega_B \sim \omega_d$ (middle panel) and for iii) $\omega_B > \omega_d$ (right panel). Inset of all graphics in this figure: $-\Delta S$ in units of k_B as a function of temperature for : i) $\omega_B < \omega_d$ (left panel) ii) $\omega_B \sim \omega_d$ (middle panel) and for iii) $\omega_B > \omega_d$ (right panel). For all graphics presented in this figure we have selected the value of $\hbar\omega_d \sim 3.6$ meV (i. e. $\omega_d = 8.7941 \times 10^{11}\ s^{-1}$).

For the MCE observable ΔT, in coherence with the values of $-\Delta S$, we obtain a mayor increase at higher values of the external magnetic field. At a field value of $B = 15.0\ T$ we approximately get ΔT of 1.5 K (in absolute value). This can be appreciated in the right panel of Fig. 8. We recall that we obtain an inverse MCE due to the strong degeneracy of this problem and is in concordance with the result previously discussed for the case of the Landau problem with degeneracy.

3.3. MCE for electrons with spin trapped in a quantum dot

In this case, the entropy has the following form as displayed in Eq. (12)

$$\frac{S_{dS}(T,B)}{k_B} = \frac{S_d(T,B)}{k_B} + \ln\left(2\cosh\left(\frac{\hbar\omega_B}{2k_BT}\right)\right) - \frac{\hbar\omega_B}{2k_BT}\tanh\left(\frac{\hbar\omega_B}{2k_BT}\right), \tag{29}$$

where $\frac{S_d(T,B)}{k_B}$ is given by Eq. (28). We can see two new terms in the last expression for the entropy when comparing to the previous case Eq. (28). These terms as compared with the previous case, these terms represent the paramagnetic contribution to the entropy arising from the spin coupled to the magnetic field. We will see below that they play a fundamental role in the results for the MCE. As the entropy of a paramagnet vanishes as a function of magnetic field at any finite temperature, the behaviour of $-\Delta S$ will be always positive for the paramagnetic contribution.

In the Fig. 9 we show the entropy (Eq. (29)) ,magnetization (from Eq. (22)) and specific heat (from Eq. (21)) as a function of Temperature. We see in such figure different behaviours of these thermodynamic quantities as a function of temperature for different magnetic field ranges. We considered three different characteristic dot frequencies as we did before in case of the spinless electron in the quantum dot. In the middle panels we consider the characteristic dot frequency of $\omega_d = 8.7941 \times 10^{11} s^{-1}$ whose value can be assimilated as a cyclotron frequency for $B = 5\ T$ (i.e. $\omega_B = 1.76 \times 10^{11} B\ \ s^{-1}$). For the superior panel of the Fig. 9 we use the value $\frac{\omega_d}{4}$,and for the figures in the bottom panels the values of $4\omega_d$ for the characteristic frequencies of the dot structure, respectively. The insets show the same quantities in an extended temperature range, from $T = 0\ K$ to $T = 50\ K$.

Preprints (www.preprints.org) | NOT PEER-REVIEWED | Posted: 2 July 2018 doi:10.20944/preprints201807.0010.v1

Peer-reviewed version available at Entropy 2018, 20, 557; doi:10.3390/e20080557

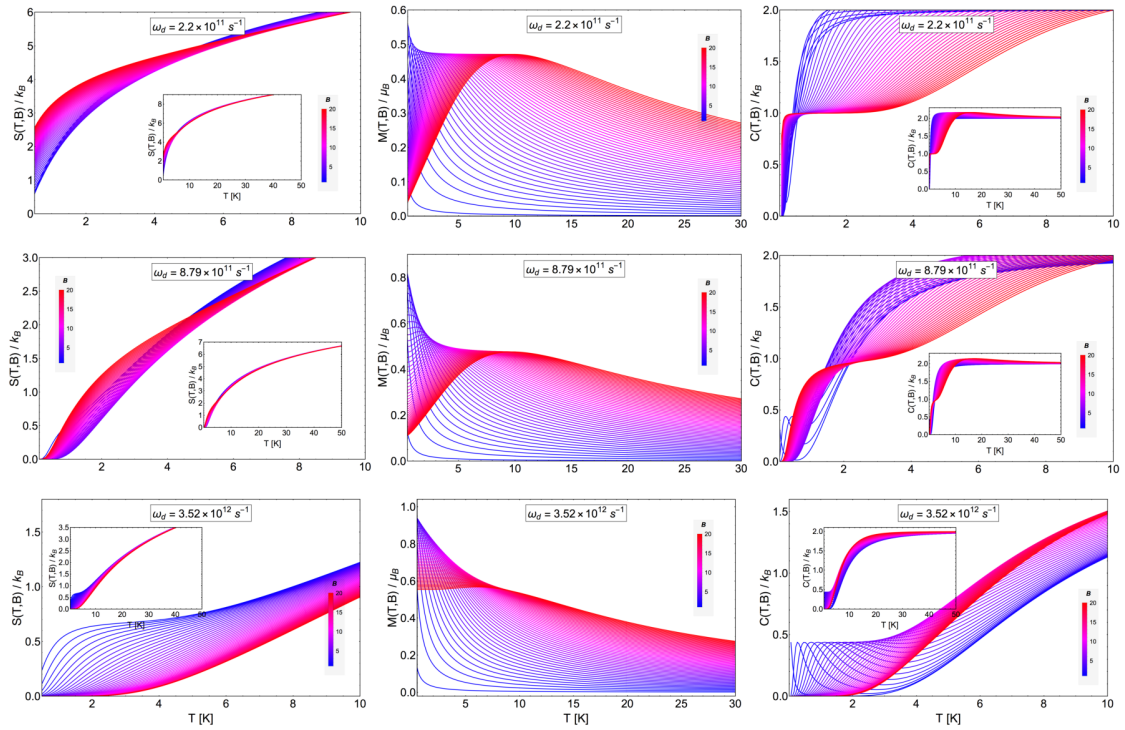

Figure 9. Electrons with spin trapped in a quantum dot. Entropy $S_{dS}(T,B)$ (left panel), $M(T,B)$ (middle panel) and $C_B(T,B)$ (right panel) as function of temperature (T) from 0 K to 10 K for different values of magnetic field in the range of 0.1 T to 20 T. In the middle panels of the graphs, we selected the representative value for the characteristic frequency of the harmonic trap in $\omega_d = 8.7941 \times 10^{11}\ s^{-1}$, which in terms of energy represents an approximately value of 3.6 meV. For the superior panels, we use the value $\frac{\omega_d}{4}$ and in the bottom panels the case of $4\omega_d$ for the characteristic frequency of the dot structure is used. The insets show the thermodynamic quantities in an extended temperature range from $T = 0\ K$ to $T = 50\ K$.

In the Fig. 10, we show the quantity $-\Delta S_{dS}$ for three characteristic dot frequencies ω_d. We clearly observe a transition for $-\Delta S_{dS}$, from positive to negative and back to positive values indicating that we have different MCE effects.

We also see the interesting effect that characteristic dot frequency plays in the transition between the direct MCE $(\Delta T > 0)$ to the inverse behaviour of the MCE $(\Delta T < 0)$. For the lower values of ω_d, (left and middle panel in the Fig. 10) a transition (change of sign) occurs at low temperatures. For the high value of ω_d, we do not get a sign change and therefore always obtain the normal MCE, (in the considered experimental range for the external magnetic fields). Aforementioned effect provides a form to controlling the type of MCE. If we focus on the results of the central panel of Fig. 10, corresponding to $\hbar\omega_d \sim 3.6\ meV$, we observe that the transition from normal to the inverse case occurs not for all magnetic field values. Under 15 T we do not observe an inverse MCE. Above 15 T we get two zero points for the difference $-\Delta S_{dS}$ and therefore a small temperature region with inverse MCE. For example, when we calculate the entropy difference between to $B_f = 20\ T$ and $B_i = 0.01\ T$, the inverse MCE region obtained is approximately between 1.1 K to 4.6 K at temperature. This can be better understood if we plot the function $S_{dS}(T,B)$ for the two magnetic fields under discussion: $S_{dS}(T,0.01)$ and $S_{dS}(T,20)$, as can be appreciated in the Fig. 11.

Preprints (www.preprints.org) | NOT PEER-REVIEWED | Posted: 2 July 2018 doi:10.20944/preprints201807.0010.v1

Peer-reviewed version available at Entropy 2018, 20, 557; doi:10.3390/e20080557

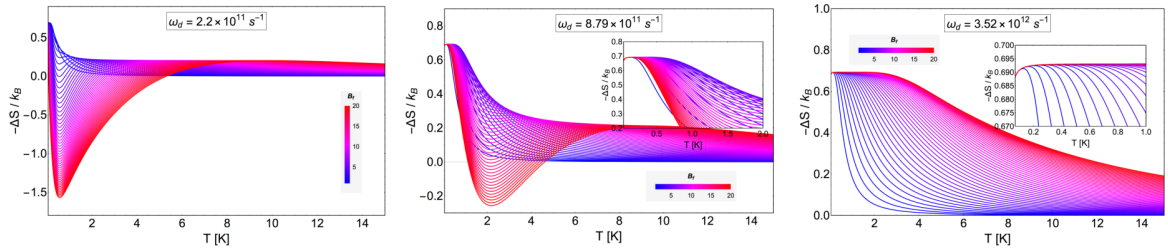

Figure 10. -$\frac{\Delta S_{dS}}{k_B}$ as a function of of temperature for different values of characteristic dot frequencies. The middle panel correspond to a value of $\omega_d = 8.7941 \times 10^{11}\ s^{-1}$. For the left panel we selected the value of $\frac{\omega_d}{4}$ and for the right panel the value of $4\omega_d$. The range of the external magnetic field values, B_f, are between 0.01 T and 20 T, and $B_i = 0.01T$. The temperature range is from $T = 0.01\ K$ to $T = 15\ K$.

In Fig. 11 we appreciate the different regions that we obtain for $-\Delta S$ for the characteristic dot frequency of 3.6 meV. The entropy for low magnetic field is not always greater than the corresponding at higher magnetic field. Between $T = 0.01\ K$ to $T = 1\ K$ we have that $S_{dS}(T, 0.01) > S_{dS}(T, 20)$, then approximately from $T = 1.2K$ to $T = 4.6\ K$ we have that $S_{dS}(T, 0.01) < S_{dS}(T, 20)$ and finally from $T = 4.7\ K$ onwards, we have the behaviour $S_{dS}(T, 0.01) > S_{dS}(T, 20)$.

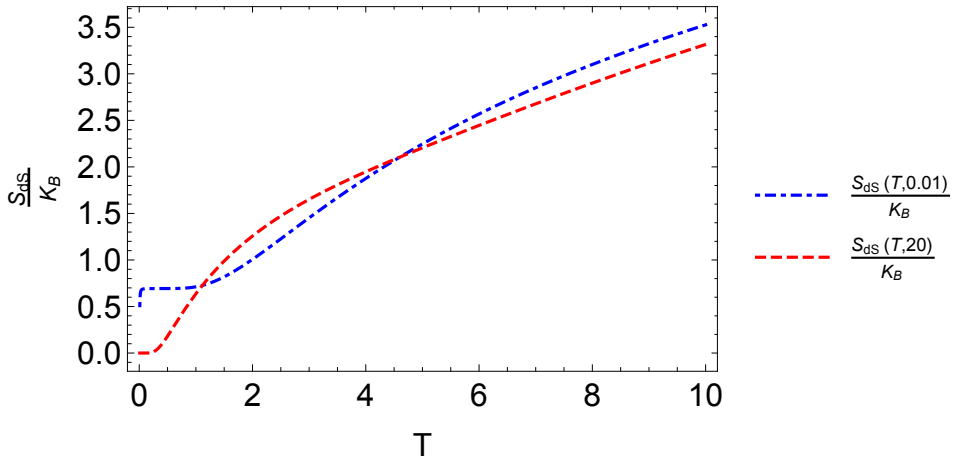

Figure 11. Entropy function $S_{dS}(T, B)$ of an electron with spin trapped in a quantum dot. We plot the entropy for two different values of the external magnetic field as a function of temperature. We use the characteristic value of $\omega_d = 8.7941 \times 10^{-11}\ s^{-1}$. Dot-dashed line corresponds to the external magnetic field $B = 0.01\ T$ and the dashed line corresponds to the value of $B = 20\ T$.

Finally, in the Fig. 12 we display ΔT as a function of temperature. The three panel are in coherence with the values of $-\Delta S$ as shown in the Fig. 11. We clearly see the behaviour of ΔT from positive to negative and back to positive values as a function of temperature (left and middle panels). In particular, we highlight the central panel, that shows a peak for ΔT with a value of approximately $\Delta T = 2.5\ K$. This peak is higher as the value of the characteristic frequency of the dot increases as we see for the extreme value for $\hbar\omega_d$ close to 12 meV in units of energy.

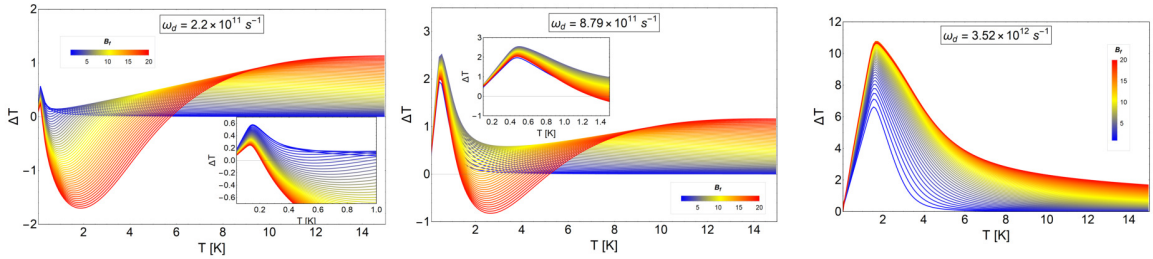

Figure 12. MCE effect for electrons with spin trapped in a quantum dot. ΔT as a function of temperature for different values of characteristic frequencies. The middle panel corresponds to a value of $\omega_d = 8.7941 \times 10^{11}\ s^{-1}$. Left panel corresponds to the value of $\frac{\omega_d}{4}$ and the right panel depicts the results using the value of $4\omega_d$. The range of the external magnetic field values, B_f, are between 0.01 T and 20 T, and $B_i = 0.01T$. The temperature range is from $T = 0.01$ K to $T = 15$ K. The insets show ΔT values zoomed in a smaller range of temperatures.

4. Conclusions

In this work, we explored the MCE for non-degenerate and degenerate Landau problem and for an ensemble of non-interacting electrons (with and without intrinsic spin) where each one is trapped inside a semiconductor quantum dot modelled by a parabolic potential. We analysed all the thermodynamics quantities and obtained the variation of entropy and the temperature along the adiabatic strokes that characterize the MCE. In particular, we focused our investigation on the role of the degeneracy effects in MCE, finding that a strong degeneracy is related to an inverse MCE.

Finally, we showed that the inclusion of the spin term allowed us to find transitions of the MCE, from normal to the inverse case due to the competition between the diamagnetism (case without spin) and the additional terms associated to paramagnetism (the case with spin). In terms of the degeneration, we expected this result, due to Zeeman split into the energy levels decreasing the degeneracy of the energy levels involved in the study, so the results must converge to normal MCE. Additionally, we can modify the characteristic frequency of the dots, to obtain a particular type of MCE (normal or inverse) allowing their use for a specific physical application (cooling or heating up).

It is important to note that our approach must be refined to take into account a many-electron scenario, which yields a more precise model. However, the non-interacting electron case is important due to its simplicity and the arising of a rich physics for comparatives cases. Moreover, this problems can be easily extended, for example, taking into account edge states and considering spin-orbit coupling for a more realistic approach.

Acknowledgments: Francisco J. Peña acknowledges the financial support of FONDECYT-postdoctoral 3170010. P. Vargas acknowledge support from Financiamiento Basal para Centros Científicos y Tecnológicos de Excelencia, under Project No. FB 0807 (Chile), P. Vargas acknowledges USM-DGIIP grant number PI-M-17-3 (Chile), O. Negrete acknowledges PIIC program number 024/2014 from USM-DGIIP, J. M. Florez acknowledges USM-DGIIP.

Author Contributions: O. Negrete, Francisco J. Peña and P. Vargas conceived the idea and formulated the theory. O. Negrete built the computer program and edited the figures. Francisco J. Peña wrote the first version of the paper. J. M. Florez contributed with discussions in the writing and edition of the same. All authors have read and approved the final manuscript.

Conflicts of Interest: The authors declare no conflict of interest.

References

1. Warburg, E. Magnetische Untersuchungen. Ueber einige Wirkungen der Coërcitivkraft. *Ann. Phys. (Leipzig)* **1881**, *249*: 141–164.
2. Weiss, P.; Piccard, A. Le pheénoméne magnétocalorique. *J. Phys. (Paris)* **1917**, *7*:103–109.
3. Weiss, P.; Piccard, A. Sur un nouveau phénoméne magnétocalorique. *Comptes Rendus* **1918**, *166*: 352–354.
4. Debye, P. Einige Bemerkungen zur Magnetisierung bei tiefer Temperatur. *Annals of Physics* **1926**, *81*: 1154–60.

5. Giauque, W. F.; Macdougall, D. P. The Production of Temperatures below One Degree Absolute by Adiabatic Demagnetization of Gadolinium Sulfate. *Journal of the American Chemical Society* **1935**, *57*, 1175–1185.
6. Brown, G. V. Magnetic heat pumping near room temperature. *Journal of Applied Physics* **1976**, *47*, 3673–3680 (1976).
7. Pecharsky, V. K.; Gschneidner, K. A. Jr. Giant Magnetocaloric Effect in Gd5(Si2Ge2). *Phys. Rev. Lett.* **1997**, *78*, 4494–4497.
8. Pathak, A.; K., Gschneidner, K. A.; Pecharsky, V. K. Negative to positive magnetoresistance and magnetocaloric effect in Pr0.6Er0.4Al2. *Journal of Alloys and Compounds* **2015**, 621, 411-414.
9. Florez, J. M.; Vargas, P.; Garcia, C.; Ross, C. A. *J. Phys. Condens. Matter* **2013**, *25* (22):226004.
10. Hudl, M.; Campanini, D.; Caron, L.; Hoglin, V.; Sahlberg, M.; Nordblad, P.; Rydh, A. Thermodynamics around the first-order ferromagnetic phase transition of Fe2P single crystals. *Phys. Rev. B* **2014**, *90 (14)*, 144432.
11. Miao, X. F.; Caron, L.; Roy, P.; Dung, N. H.; Zhang, L.; Kockelmann, W. A.; *et. al.* Tuning the phase transition in transition-metal-based magnetocaloric compounds. *Phys. Rev. B* **2014**, *89 (17)*, 174429-6.
12. Sosin, S.; Prozorova, L.; Smirnov, A.; Golov, A.; Berkutov, I.; Petrenko, O.; *et al.* Magnetocaloric effect in pyrochlore antiferromagnet Gd2Ti2O7. *Phys. Rev. B* **2005**, *71 (9)*, 2005094413.
13. Wang, F.; Yuan, F.-Y.; Wang, J.-Z.; Feng, T.-F.; Hu, G.-Q. Conventional and inverse magnetocaloric effect in Pr2CuSi3 and Gd2CuSi3 compounds. *Journal of Alloys and Compounds* **2014**, *592*, 63-66.
14. Du, Q.; Chen, G.; Yang, W.; Wei, J.; Hua, M.; Du, H.; *et al.* Magnetic frustration and magnetocaloric effect in AlFe2-x Mn x B2 (x = 0-0.5) ribbons. *Journal of Physics D-Applied Physics* **2015**, *48* (33), 335001.
15. Balli, M.; Fruchart, D.; Zach, R. Negative and conventional magneto- caloric effects of a MnRhAs single crystal. *Journal of Applied Physics* **2014**, *115 (20)*, 203909.
16. Kolat, V. S.; Izgi, T.; Kaya, A. O.; Bayri, N.; Gencer, H.; Atalay, S. Metamagnetic transition and magnetocaloric effect in charge-ordered Pr0.68Ca0.32- xSrxMnO3 (x=0, 0.1, 0.18, 0.26 and 0.32) compounds. *Journal of Magnetism and Magnetic Materials* **2010**, *322 (4)*, 427433 .
17. Phan, M. H.; Morales, M. B.; Bingham, N. S.; Srikanth, H.; Zhang, C. L.; Cheong, S.-W. Phase coexistence and magnetocaloric effect in $La_{5/8}$-y Pry $Ca_{3/8}$ MnO_3(y= 0.275). *Phys. Rev. B* **2010**, *81 (9)*, 094413.
18. Patra, M.; Majumdar, S.; Giri, S.; Iles, G. N.; Chatterji, T. Anomalous magnetic field dependence of magnetocaloric effect at low temperature in Pr0.52Sr0.48MnO3 single crystal. *Journal of Applied Physics* **2010**, *107 (7)*, 6101.
19. Szalowski, K.; Balcerzak, T. Normal and inverse magnetocaloric effect in magnetic multilayers with antiferromagnetic interlayer coupling. *Journal of Physics Condensed Matter* **2014**, *26 (38)*, 386003.
20. Midya, A.; Khan, N.; Bhoi, D.; Mandal, P. Giant magnetocaloric effect in magnetically frustrated $EuHo_2O_4$ and $EuDy_2O_4$ compounds. *Applied Physics Letters* **2012**, *101 (13)*, 132415 .
21. Moya, X.; Kar-Narayan, S.; Mathur, N. D. Caloric materials near ferroic phase transitions. *Nature Materials* 2014, *13 (5)*, 439-450.
22. Guillou, F.; Porcari, G.; Yibole, H.; van Dijk, N.; Bruck, E. Taming the First-Order Transition in Giant Magnetocaloric Materials. *Advanced Materials* **2014**, *26 (17)*, 2671-2675.
23. Gong, Y.-Y.; Wang, D.-H.; Cao, Q.-Q.; Liu, E.-K.; Liu, J.; Du, Y.-W. Electric Field Control of the Magnetocaloric Effect. *Advanced Materials* **2014**, *27 (5)*, 801-805.
24. Nalbandyan, V. B.; Zvereva, E. A.; Nikulin, A. Y.; Shukaev, I. L.; Whangbo, M.- H.; Koo, H.-J.; *et al.* New Phase of $MnSb_2O_6$ Prepared by Ion Exchange: Structural, Magnetic, and Thermodynamic Properties. *Inorganic Chemistry* **2015**, *54 (4)*, 1705-1711.
25. Tkac, V.; Orendacova, A.; Cizmar, E.;, Orendac, M.; Feher, A.; Anders, A. G. Giant reversible rotating cryomagnetocaloric effect in $KEr(MoO_4)_2$ induced by a crystal-field anisotropy. *Phys. Rev. B* **2015**, *92 (2)*, 024406-5.
26. Tamura, R.; Ohno, T.; Kitazawa, H. A generalized magnetic refrigeration scheme. *Applied Physics Letters* **2014**, *104 (5)*, 052415-5.
27. Tamura, R.; Tanaka, S.; Ohno, T.; Kitazawa, H. Magnetic ordered structure dependence of magnetic refrigeration efficiency. *Journal of Applied Physics* **2014**, *116 (5)*, 053908-13.
28. Li, G.; Wang, J.; Cheng, Z.; Ren, Q.; Fang, C.; Dou, S. Large entropy change accompanying two successive magnetic phase transitions in $TbMn_2Si_2$ for magnetic refrigeration. *Applied Physics Letters* **2015**, *106 (18)*, 182405.

29. Peña F. J.; González, A.; Nunez A. S.; Orellana P. A.; Rojas, R. G.; Vargas, P. Magnetic Engine for the Single-Particle Landau Problem. *Entropy* **2017**, *19 (12)*, 639.
30. Mani, R.G.; Smet, J.H.; von Klitzing, K.; Narayanamurti, V.; Johnson, W.B.; Umansky, V. Zero-resistance states induced by electromagnetic-wave excitation in GaAs/AlGaAs heterostructures. *Nature* **2002**, 420, 646-650.
31. Prance, J. R.; Smith, C. G.; Griffiths, J. P.; Chorley, S. J.; Anderson, D.; Jones, G. A. C.; Farrer, I.; Ritchie, D. A. Electronic Refrigeration of a Two-Dimensional Electron Gas. *PRL* **2009**, *102*, 146602.
32. Hübel, A.; Held, K.; Weis, J.; Klitzing, K. v. *Phys. Rev. Lett.* **2008**, *101*, 186804 (2008).
33. Hübel, A.; Weis, J.; Dietsche, W.; Klitzing, K. v. Two laterally arranged quantum dot systems with strong capacitive interdot coupling. *Appl. Phys. Lett.* **2007**, *91*, 102101.
34. Donsa, S.; Andergassen S.; Held, K.; Double quantum dot as a minimal thermoelectric generator. *Phys. Rev. B* **2014**, *89*, 125103.
35. Muñoz, E.; Peña, F.J.; González, A. Magnetically-Driven Quantum Heat Engines: The Quasi-Static Limit of Their Efficiency. *Entropy* **2016**, *18*, 173.
36. Muñoz, E.; Peña, F.J. Magnetically driven quantum heat engine. *Phys. Rev. E* **2014**, *89*, 052107.
37. Peña, F.J.; Muñoz, E. Magnetostrain-driven quantum heat engine on a graphene flake. *Phys. Rev. E* **2015**, *91*, 052152.
38. Kumar, J.; Sreeram, P.A.; Dattagupta, S. Low-temperature thermodynamics in the context of dissipative diamagnetism. *Phys. Rev. E* **2009**, *79*, 021130.